The 2019 World Congress on
Advances in Structural Engineering and Mechanics (ASEM19)
Jeju Island, Korea, September 17 - 21, 2019

The near wake of three circular cylinders in an equilateral triangular arrangement at Re = 100

*Honglei Bai[1)], Yufeng Lin[2)] and Md. Mahbub Alam[3)]

[1)] *School of Aeronautics and Astronautics, Sun Yat-sen University, Shenzhen, China*
[2)] *WSP (Asia) Ltd, Kowloon Bay, Kowloon, Hong Kong SAR, China*
[3)] *Institute for Turbulence-Noise-Vibration Interaction and Control, Harbin Institute of Technology, Shenzhen, China*
[1)] *hl_bai@126.com, baihlei3@mail.sysu.edu.cn*

ABSTRACT

Two-dimensional numerical simulations are conducted at a low Reynolds number Re = 100 to investigate the near wake of three identical circular cylinders which are arranged in an equilateral triangular configuration. The incident angle of the three-cylinder configuration with respect to incoming flow is changed from $\theta = 0^o$ to 60°, while the spacing between adjacent cylinders (L) covers a wide range of L/D = 1.25-7.0, where D is diameter of the cylinder. It has been observed that flow structures in the near wake of the three-cylinder configuration, time-mean and fluctuating fluid forces on the individual cylinders strongly depend on (L/D, θ). The three-cylinder configuration generates a single Karman vortex street, a deflected near wake, or two or three streets of vortices in the near wake, depending on (L/D, θ). Furthermore, there is a close correlation between the near wake behaviour and the fluid forces observed.

1. INTRODUCTION

Multiple bluff bodies in proximity have been frequently seen in practical engineering applications such as high-rise buildings, bridge piers, heat exchangers and offshore platforms. Flow around these multiple bluff bodies involves boundary layer development, flow separation, shear layer oscillation, fluid structure interaction, vortex dynamics, and so on (e.g., Alam, Bai & Zhou 2016). A circular cylinder is the basic model of a bluff body, and thus a pair of circular cylinders and a group of three circular cylinders have been considered as the representative model of multiple bluff bodies (e.g., Zadravkovich 1997; Zhou & Alam 2016). While the flow around a pair of circular cylinders has been extensively studied, both experimentally and numerically (Zhou & Alam 2016), that around a group of three circular cylinders has received little attention

---

[1)] Associate Professor
[2)] Senior Engineer
[3)] Full Professor

in the literature.

The simplest configuration for a group of three circular cylinders is that the cylinders are placed in an equilateral triangular arrangement. As such, the configuration is determined by two parameters, i.e., the spacing between the centers of adjacent cylinders (*L*) and the incident angle of the three-cylinder configuration with respect to the incoming flow (θ). For the convenience of following discussion, $\theta = 0^o$ is defined as the configuration that one cylinder (labeled as cylinder 1) is located upstream while the other two cylinders (labeled as cylinder 2 and cylinder 3 in a clockwise direction) are located downstream and in a side-by-side manner that is symmetric about a horizontal line going through the center of cylinder 1. In this way, at $\theta = 30^o$ cylinder 1 and cylinder 2 are in a tandem arrangement with cylinder 3 on the side, and at $\theta = 60^o$ cylinder 1 and cylinder 3 are side-by-side and located upstream of cylinder 2.

Flow structures around the three cylinders are strongly dependent on their geometrical configuration that is determined by *L* and θ. Lam & Cheung (1988), using dye flow visualization, investigated flow patterns around a group of three cylinders at a lower subcritical Reynolds number range Re = $U_\infty D/\nu$ = (2.1-3.5) × 10^3, where U_∞ is the incoming velocity of free stream, *D* is diameter of the cylinder and ν is the kinematic viscosity of fluid. The three-cylinder configuration considered in their work covers L/D = 1.27-5.43 and $\theta = 0^o$-60° (with an interval of 10°). At $\theta = 0^o$, bistable biased base flow downstream of the side-by-side cylinders 2 and 3 was observed at small spacing L/D < 2.29. At $\theta = 60^o$, the upstream side-by-side cylinders 1 and 3 generated narrow near wakes with a higher frequency of vortex shedding while the downstream cylinder 2 produced a wide near wake with a lower frequency of vortex shedding. Wake interference occurred at other incident angles. For example, at $\theta = 30^o$ cylinder 2 was submerged in the wake of the upstream cylinder 1, but the wake interference was influenced by the presence of the third cylinder located on the side. The bistable biased base flow downstream of the side-by-side cylinders 2 and 3 was also observed by Tatsuno et al. (1998) in smoke flow visualization at $\theta = 0^o$ and L/D < 1.73 (Re = 507). Regarding the influence of spacing on the flow (Re = 1.4-5.5 × 10^4), Gu & Sun (2001) identified four different regimes, i.e., effects of small ($1.7 \leq L/D \leq 2.2$), transition ($L/D = 2.2$), medium ($2.5 \leq L/D \leq 3.0$) and large spacing ($L/D \geq 4.0$), and classified three basic types of interference at the small spacing ($1.7 \leq L/D \leq 2.2$), i.e., interference of proximity, shear layer reattachment and wake. The interference of proximity and wake was observed in the small and large spacing, respectively, by Bao et al. (2010), based on two-dimensional numerical simulations at a low Re = 100 ($1.5 \leq L/D \leq 5.0$, $\theta = 0^o$, 30° and 60°). Furthermore, they noted that the flow patterns were influenced by both the interference of proximity and wake when the spacing of adjacent cylinders is intermediate. These interference effects and flow patterns were also identified when the three cylinders were elastically supported individually (Wang et al. 2013; Re = 150; $L/D = 5.0$ and $\theta = 0^o$, 30° and 60°) or as a rigidly coupled group (Han et al. 2018; Re = 10^3-3 × 10^4; $L/D = 4.0$ and $\theta = 0^o$, 15°, 30°, 45° and 60°).

Fluid forces acting on the individual cylinders are closely associated with the behavior of flow structures around the three-cylinder configuration. Based on the drag and lift forces obtained from surface pressure distributions (Re = 6.2 × 10^4), Tatsuno et al. (1998) found that, at $\theta = 0^o$ and L/D < 1.73, the drag or lift forces on the

downstream side-by-side cylinders 2 and 3 were not always identical for the two cylinders, which is ascribed to the unsteady behavior of the bistable base flow. Gu & Sun (2001) found that, at θ = 20°-30° and medium and large spacing, the time-mean drag and lift forces on cylinder 2 was minimum. This is because cylinder 2 was partially or totally submerged in the wake of the upstream cylinder 1 in the configurations. They also noted that the reattachment of shear layer on the downstream cylinder yielded a significant lateral force on the cylinder.

This work aims to conduct a systematic numerical study on the flow structures and fluid forces of the three cylinders arranged in an equilateral triangular form. Two-dimensional numerical simulations are carried out at a low Re = 100 in the laminar flow regime. The spacing *L* and incident angle θ cover a wide range, i.e., *L/D* = 1.25-7.0 with an increment of 0.25 or 0.5, and θ = 0°-60° with an increment of 5°. Numerical simulation details are given in section 2. Typical flow structures and fluid forces are discussed in section 3 and 4, respectively. This work is concluded in section 5.

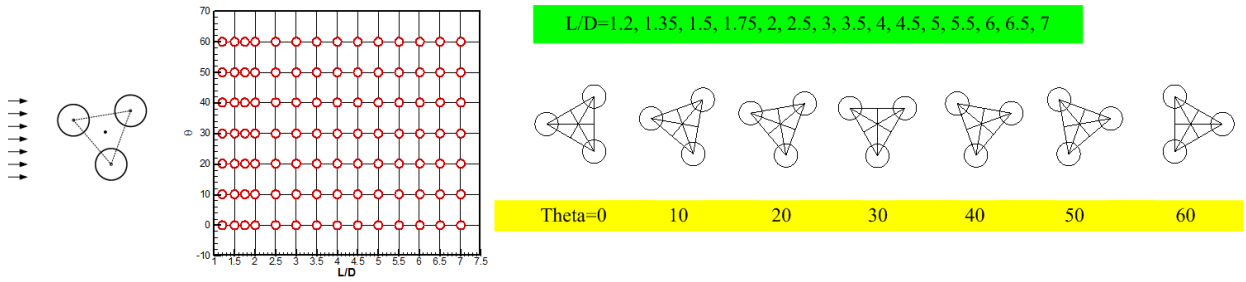

Fig. 1 Configurations of three circular cylinders in an equilateral triangular arrangement. θ denotes the incident angle of the three-cylinder configuration with respect to incoming flow, and *L/D* is the spacing between adjacent cylinders normalized by the cylinder diameter *D*.

2. NUMERICAL SIMULATION DETAILS

Figure 1 shows the schematic of three circular cylinders in an equilateral triangular arrangement. The three cylinders have an identical diameter *D*. The spacing between adjacent cylinders is *L*. The incident angle of the three-cylinder configuration with respect to the incoming flow direction is denoted by θ. θ is increased when the three-cylinder configuration is rotated about its center in a clockwise direction. Due to symmetry, θ = 0°-60° covers all possible orientations of such a three-cylinder configuration. *L/D* = 1.25, 1.5, 2.0, 2.5, 3.0, 3.5, 4.0, 4.5, 5.0, 5.5, 6.0, 6.5 and 7.0. The grid dots in the (*L/D*, θ) plane indicate all the configurations of the three cylinders considered in this work.

Two-dimensional numerical simulations are conducted at a low Re = 100 to investigate the unsteady laminar flow around the three cylinders. The two-dimensional incompressible Navier-Stokes (N-S) equations are solved using the finite-volume method in ANSYS Fluent. The continuity and N-S equations governing the flows can be written in the Einstein convention as below

$$\frac{\partial u_i}{\partial x_i} = 0,$$

$$\frac{\partial u_i}{\partial t} + \frac{\partial u_i u_j}{\partial x_j} = -\frac{1}{\rho}\frac{\partial p}{\partial x_i} + \nu \frac{\partial^2 u_i}{\partial x_j \partial x_j},\ i \in \{1,2\},$$

where t denotes time, x_i are the Cartesian coordinates (i.e., x_1 and x_2 denote the streamwise x- and cross-stream y-directions, respectively), u_i are the velocity components along the corresponding x_i, p is the fluid pressure and ρ is the fluid density.

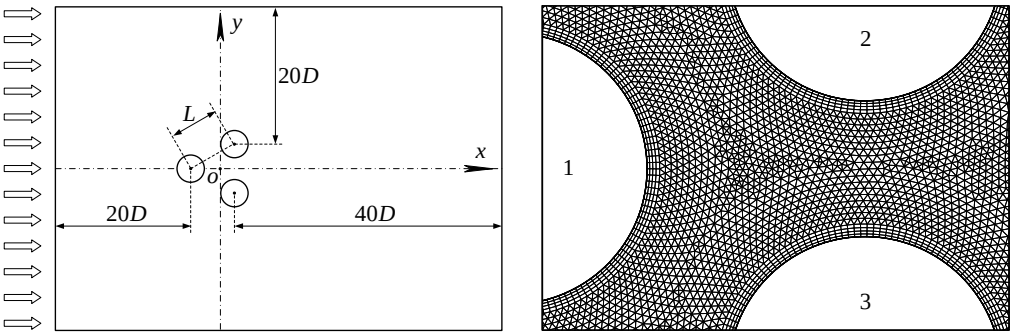

Fig. 2 Computation domain (left) and mesh details around the three cylinders (right).

As shown in Fig. 2, the computational domain around the three cylinders is a rectangle. The upstream inlet of the computation domain is 20*D* far away from the most upstream cylinder, while the downstream outlet of the computational domain is 40*D* far away from the most downstream cylinder. The lateral sides of the computational domain have a distance of 20*D* from the cylinder on each side of the symmetric line. The size of the computational domain is accordingly changed when the three-cylinder configuration is changed at different (*L*/*D*, θ). The entire computational domain is divided into two zones to facilitate mesh generation. One of them is a circle co-centered with the three-cylinder configuration and covering all the three cylinders. The mesh generated within this zone is unstructural triangular grids. However, to ensure accurate prediction of fluid forces on the individual cylinders, structural quadrilateral meshes are generated immediately around the cylinders, with the nearest grid having 0.01*D* from the cylinder surface, and stretched radially by a ratio of 1.2 and a total of 5 layers. The outside zone of the computational domain is meshed by quadrilateral grids. The total number of grids in the entire computational domain ranges from 105070 to 110260, depending on the three-cylinder configuration.

A uniform streamwise velocity (i.e., U_∞) is imposed at the inlet boundary, while a pressure-outlet boundary condition is used in the outlet boundary. The 'no-slip' boundary condition is applied to the cylinder surface. The lateral sides are treated as slip sides using symmetric conditions.

The pressure-velocity coupling in the governing equations is based on the algorithms of SIMPLEC. For the discretization of pressure and momentum, the second-order and second-order upwind differencing schemes are employed, respectively, while for the temporal discretization the second-order implicit differencing scheme is used.

The non-dimensional time step used in the computation is $\Delta t^* = \Delta t\, U_\infty / D$ = 0.02, yielding a CFL number < 1 in most part of the computational domain.

3. TYPICAL FLOW STRUCTURES

3.1 A single Karman vortex street

When the spacing between adjacent cylinders is small (i.e., $L/D \leq$ 1.5), the group of three cylinders behaves like a single bluff body, generating a single Karman vortex street, irrespective of the incident angle θ. Fig. 3 shows the representative flow structures for two different configurations [(*L/D*, θ) = (1.25, 0°) and (1.25, 60°)], in terms of contours of instantaneous vorticity. It can be seen that, for (*L/D*, θ) = (1.25, 0°) (Fig. 3a) shear layers separating from the upstream cylinder 1 overshoot the downstream side-by-side cylinders 2 and 3, and then roll up into a single Karman vortex street of counter-signed staggered vortices along the streamwise direction. The gap flow going through the cylinders is too weak to develop shear layers in the inner sides of the downstream side-by-side cylinders. For (*L/D*, θ) = (1.25, 60°) (Fig. 3b), where cylinder 1 and cylinder 3 are side-by-side and located upstream of cylinder 2, shear layers separating from the outer sides of the upstream cylinders 1 and 3 extend longitudinally, due to the presence of the downstream cylinder 2, and then roll up into a single Karman vortex street of counter-signed staggered vortices. In this arrangement of the three cylinders (Fig. 3b), the incoming free stream get into the narrow gap between the upstream side-by-side cylinders and get out into the base through the outlets formed by the upstream cylinders and the downstream cylinder. As a result of this, the rolling up of the shear layers into vortices is somewhat delayed, producing to a Karman vortex street of reduced shedding frequency (Lam & Cheung 1988). The group of three cylinders in Fig. 3(b) has a wider near wake than that in Fig. 3(a).

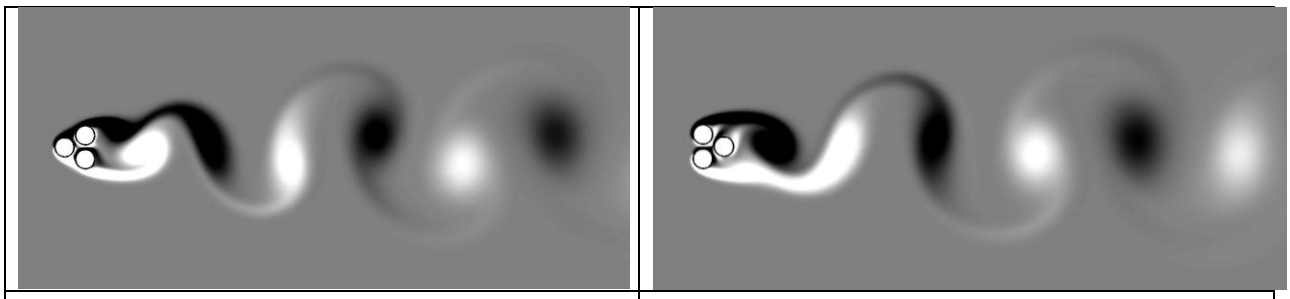

(a)	(b)

Fig. 3 Contours of instantaneous vorticity in the near wake of the three cylinders at (a) (*L/D*, θ) = (1.25, 0°) and (b) (*L/D*, θ) = (1.25, 60°). White and black colors indicate positive and negative vorticities, respectively.

3.2 A deflected near wake

When the three-cylinder configuration is asymmetric about the horizontal line going through the center of the configuration, a deflected near wake is generated

downstream of the three cylinders at the intermediate spacing ($1.5 < L/D \leq 3.0$). Fig. 4 shows the typical flow structures for two different configurations [(L/D, θ) = (2.5, 10°) and (2.5, 30°)], in terms of contours of instantaneous vorticity. At the intermediate spacing, the gap flow going through the cylinders has enough momentum to be biased in the near wake; as such the downstream cylinders may have relatively narrow and wide wakes. For (L/D, θ) = (2.5, 10°) (Fig. 4a), the near wake of the upstream cylinder 1 is completely suppressed by the downstream cylinders 2 and 3; the gap flow is biased toward the lower cylinder 3. As a result, the downstream cylinders 2 and 3 generate relatively wide and narrow wakes, respectively. Further downstream, the inner shear layers associated with the gap flow are enveloped by the vortices formed on the lower side of cylinder 3, while counter-signed vortices shed from the upper side of cylinder 2. Therefore, only a vortex street is produced, with distinct frequencies of vortex shedding from the upper and lower sides of the three-cylinder configuration.

For (L/D, θ) = (2.5, 30°) (Fig. 4b), the downstream cylinder 2 is totally submerged in the wake of the upstream cylinder 1. In other words, the shear layers separating from the upstream cylinder 1 overshoot the downstream cylinder 2 and roll up into vortices downstream of cylinder 2. However, the gap flow, which is biased toward cylinder 3, results in a relatively narrow wake for cylinder 3 and a relatively wide wake for cylinder 2. Again, the inner shear layers associated with the gap flow are enveloped by the vortices formed on the lower side of cylinder 3. Therefore, only one vortex street is generated, which is similar to the configuration with a smaller θ (Fig. 4a).

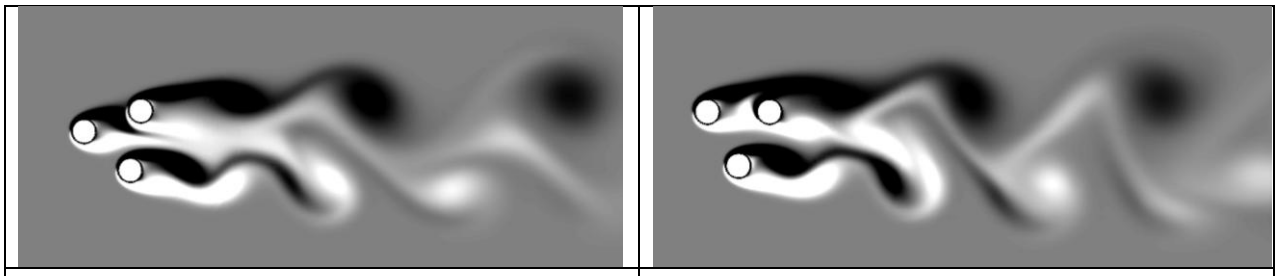

(a) (b)

Fig. 4 Contours of instantaneous vorticity in the near wake of the three cylinders at (a) (L/D, θ) = (2.5, 10°) and (b) (L/D, θ) = (2.5, 30°).

3.3 Two streets of vortices

At the large spacing $3.0 < L/D \leq 4.0$ and $\theta < 50^o$, the group of three cylinders produces a wake consisting of two streets of vortices. Fig. 5 shows the typical flow structures for two different configurations [(L/D, θ) = (4.0, 0°) and (4.0, 30°)], in terms of contours of instantaneous vorticity. For (L/D, θ) = (4.0, 0°) (Fig. 5a), the three-cylinder configuration is symmetric about the horizontal line going through the center of the configuration. The shear layers separating from the upstream cylinder 1 are confined by the downstream side-by-side cylinders 2 and 3, and thus there is no vortex rolling up in the gap. Meanwhile, each of the downstream cylinders generates a Karman vortex street, with the vortex shedding from the two cylinders appearing an

anti-phase fashion. Therefore, the pattern of counter-signed vortices appears symmetric about the horizontal line going through the center of the configuration.

For (L/D, θ) = (4.0, 30°) (Fig. 5b), cylinder 1 and cylinder 2 are in a tandem arrangement while cylinder 3 is located on the lower side of cylinders 1 and 2. The large spacing between cylinder 1 and cylinder 2 allows the upstream cylinder 1 to generate its near wake of shedding vortices. The reattachment of the vortices from the upstream cylinder 1 triggers vortices shedding from the downstream cylinder 2 and, consequently, there is one Karman vortex street downstream of the tandem cylinders 1 and 2. Cylinder 3 also produces a Karman vortex street. Therefore, this configuration of the three cylinders has a near wake of two streets of vortices.

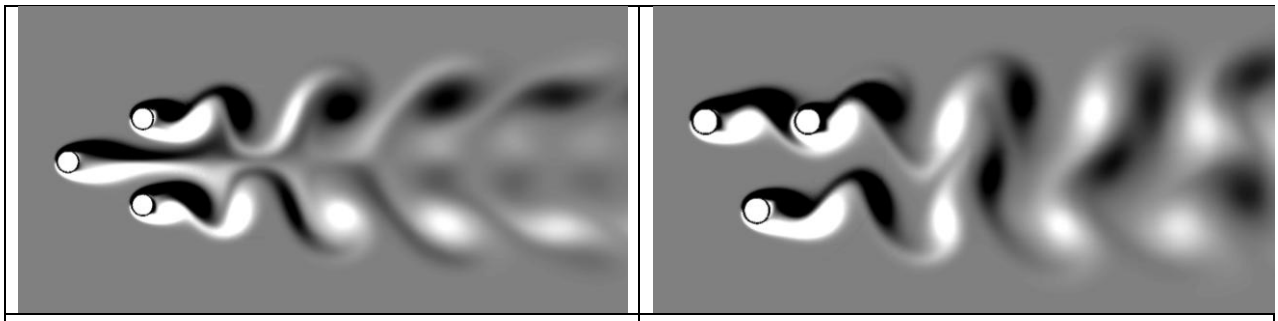

(a) (b)

Fig. 5 Contours of instantaneous vorticity in the near wake of the three cylinders at (a) (L/D, θ) = (4.0, 0°) and (b) (L/D, θ) = (4.0, 30°).

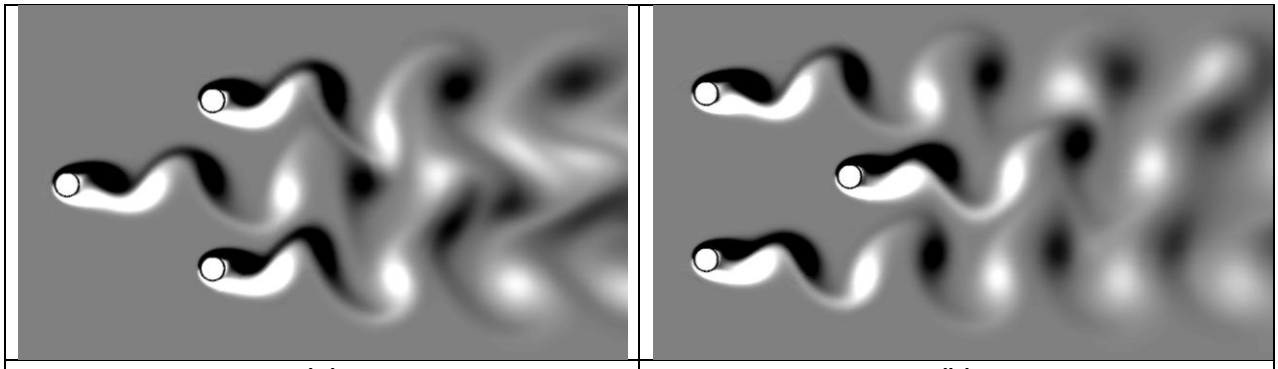

(a) (b)

Fig. 6 Contours of instantaneous vorticity in the near wake of the three cylinders at (a) (L/D, θ) = (7.0, 0°) and (b) (L/D, θ) = (7.0, 60°).

3.4 Three streets of vortices

For the symmetric configurations (θ = 0° and 60°) of the three cylinders at the large spacing $L/D >$ 4.0, a near wake of three streets of vortices is generated. Fig. 6 shows the flow structures for (L/D, θ) = (7.0, 0°) and (7.0, 60°), in terms of contours of instantaneous vorticity. It can be seen that each of the three cylinders generates a

Karman vortex street. The street of vortices in the middle interacts with the other two streets of vortices as they evolve downstream.

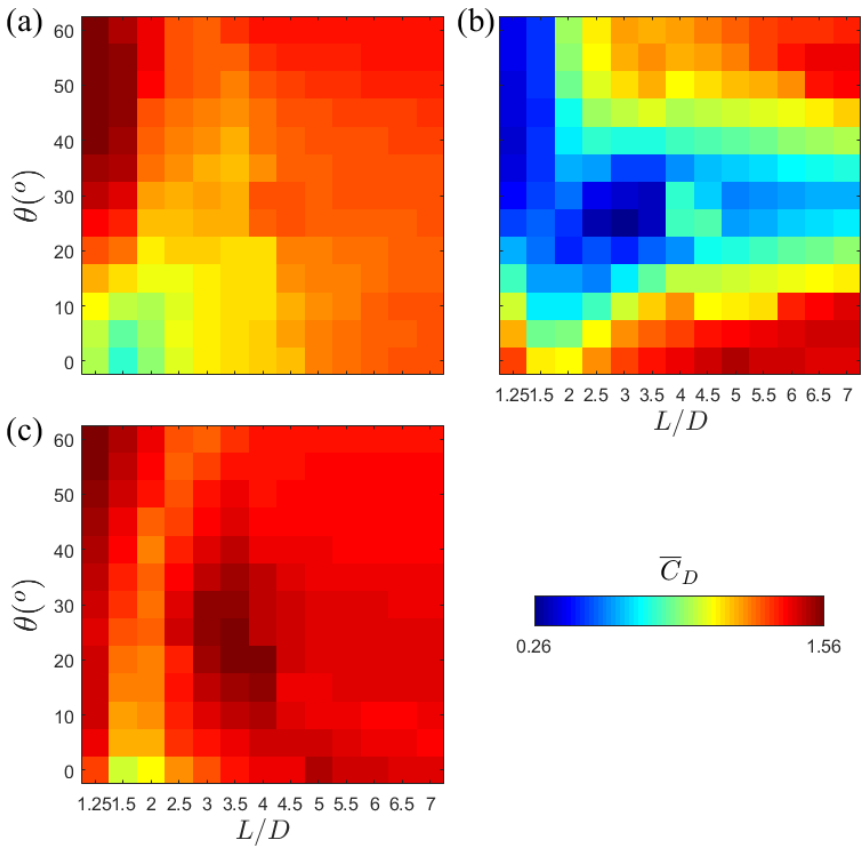

Fig. 7 Dependence of time-mean drag force ($\overline{C}_D$) on (*L/D*, θ) for cylinder 1 (a), cylinder 2 (b) and cylinder 3 (c).

4. FLUID FORCES

4.1 Time-mean forces

Time-mean drag and lift forces acting on the individual cylinders are presented in Figs. 7 and 8, respectively, in terms of contours of force coefficients in the (*L/D*, θ) plane. This provides a global view of the dependence of fluid forces on the three-cylinder configurations.

In Fig. 7, the maximum drag coefficient ($\overline{C}_D$) is identified at (*L/D*, θ) = (1.25, 50°) for cylinder 1 and at (*L/D*, θ) = (3.5, 20°) for cylinder 3, while the minimum $\overline{C}_D$ is detected at (*L/D*, θ) = (3.0, 25°) for cylinder 2.

In Fig. 8, it can be seen that cylinder 1 and cylinder 3 are associated with time-mean lift forces with large magnitude at the small spacing ($L/D <$ 1.5). The positive lift force (along the positive y-direction) is acting on cylinder 1, while the negative lift force (along the negative y-direction) is acting on cylinder 3. That is, cylinder 1 and cylinder 3 are repelled by the opposite lift forces. For cylinder 2, at the intermediate spacing 2.5

$< L/D <$ 4.0 the lift force switches from negative to positive as the incident angle θ is increase from 10° to 50°.

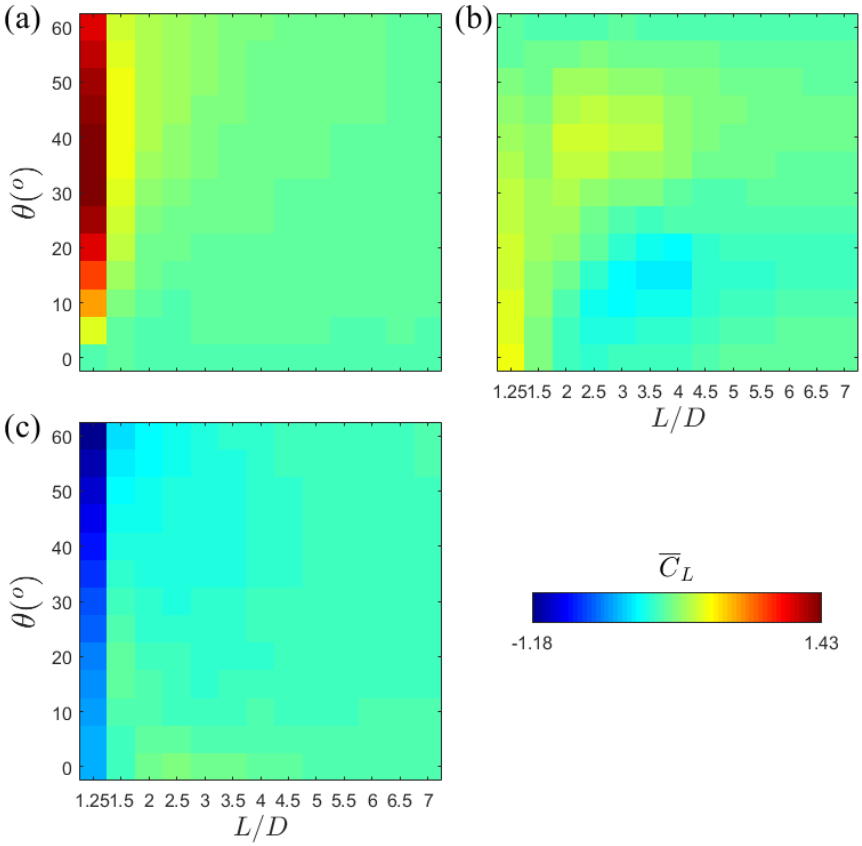

Fig. 8 Dependence of time-mean lift force ($\overline{C}_L$) on (*L/D*, θ) for cylinder 1 (a), cylinder 2 (b) and cylinder 3 (c).

4.2 Fluctuating forces

The fluctuating drag and lift forces on the three cylinders are presented Figs. 9 and 10, respectively. At the small spacing $L/D \leq$ 1.25, all three cylinders are associated with large fluctuating drag forces ($C_D^{'}$). At the large spacing $L/D >$ 4.0, there is a large fluctuating drag force on cylinder 2 throughout the range of incident angle. This cylinder is also associated with a large fluctuating lift force at the large spacing $L/D >$ 4.0 and 20° < θ < 40° (Fig. 10b).

5. CONCLUSIONS

A systematic numerical simulation study was conducted at a low Re = 100 to investigate the flow structures and fluid forces of the three cylinders arranged in an equilateral triangular form. The spacing between adjacent cylinder was from *L/D* = 1.25-7.0 while the incident angle was changed from θ = 0° to 60° (covering all possible orientation configurations). It has been observed that flow structures in the near wake

of the three-cylinder configuration, time-mean and fluctuating fluid forces on the individual cylinders strongly depend on (*L/D*, θ). The three-cylinder configuration generates a single Karman vortex street, a deflected near wake, or two or three streets of vortices in the near wake, depending on (*L/D*, θ). Furthermore, there is a close correlation between the near wake behaviour and the fluid forces observed.

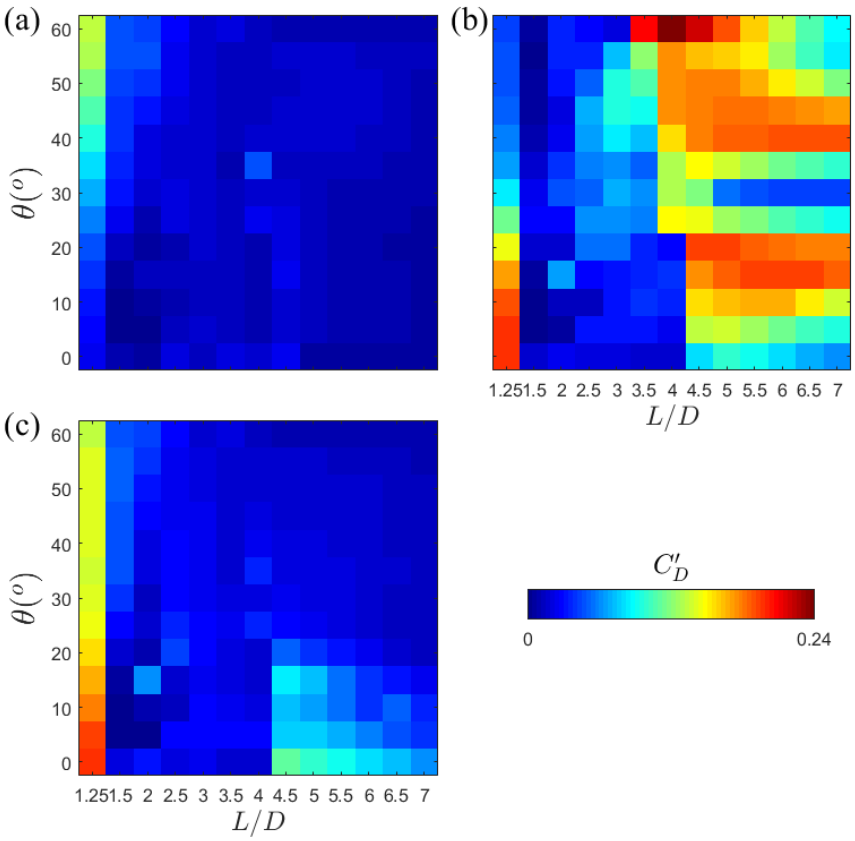

Fig. 9 Dependence of fluctuating drag force ($C_D^{'}$) on (*L/D*, θ) for cylinder 1 (a), cylinder 2 (b) and cylinder 3 (c).

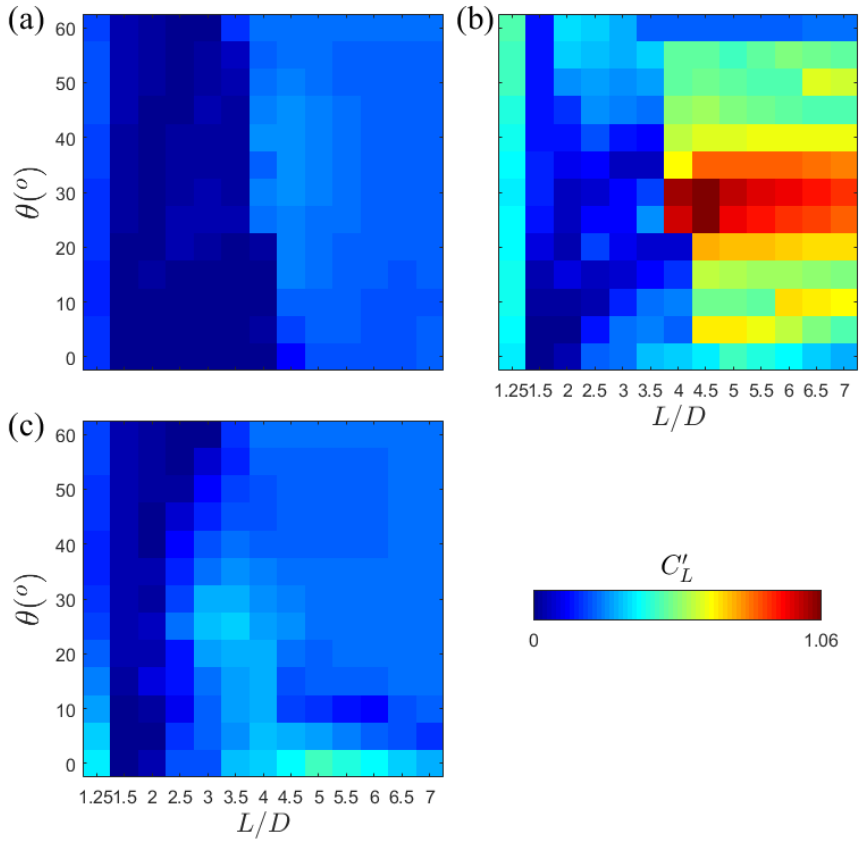

Fig. 10 Dependence of fluctuating lift force ($C_L^{'}$) on (*L/D*, θ) for cylinder 1 (a), cylinder 2 (b) and cylinder 3 (c).

REFERENCES

Alam, M.M., Bai, H.L. and Zhou, Y. (2016), "The wake of two staggered square cylinders", *J. Fluid Mech.*, **801**, 475-507.

Bao, Y., Zhou, D. and Huang, C. (2010), "Numerical simulation of flow over three circular cylinders in equilateral arrangements at low Reynolds number by a second-order characteristic-based split finite element method", *Comp. Fluids*, **39**, 882-899.

Gu, Z. and Sun, T. (2001), "Classification of flow pattern on three circular cylinders in equilateral-triangular arrangements', *J. Wind Eng. Indust. Aerodyn*. **89**, 553-568.

Han, P., Pan, G. and Tian, W. (2018), "Numerical simulation of flow-induced motion of three rigidly coupled cylinders in equilateral-triangle arrangement", *Phys. Fluids*, **30**, 125107.

Lam, K. and Cheung W.C. (1988), "Phenomena of vortex shedding and flow interference of three cylinders in different equilateral arrangements", *J. Fluid Mech.*, **196**, 1-26.

Tatsuno, M., Amamoto, H. and Ishi-I, K. (1998), "Effects of interference among three equidistantly arranged cylinders in a uniform flow", *Fluid Dyn. Research*., **22**, 297-315.

Wang, H., Yu, G. and Yang, W. (2013), "Numerical study of vortex-induced vibrations of three circular cylinders in equilateral-triangle arrangement", *Advan. Mech. Eng*., **2013**, 287923.

Zdravkovich, M.M. (1977), "Review of flow interference between two circular cylinders in various arrangements", *J. Fluids Eng*. **99**, 618-633

Zhou, Y. and Alam, M.M. (2016), "Wake of two interacting circular cylinders: A review", *Int. J. Heat Fluid Flow*, **62**, 510-537.